

$M$	= polymer amount	[kg]	$S$	= gel matrix
$Q$	= heat of phase transition	[J/(kg·s)]	$T$	= transition point
$R$	= gel radius at time $t$	[m]	$W$	= water
$r$	= radial position	[m]		
$T$	= temperature	[K]	<Superscript>	
$t$	= time	[s]	— (over bar)=	dimensionless
$\Delta t$	= time increment	[s]		
$U$	= radial velocity	[m/s]		
$V$	= gel volume	[m <sup>3</sup> ]		
$V_{\infty}$	= equilibrium gel volume	[m <sup>3</sup> ]		
$\varepsilon$	= volume fraction of water within gel	[—]		
$\rho$	= density	[kg/m <sup>3</sup> ]		
$\tau$	= dimensionless time ( $= tK_w/(\rho_w C_{PW} r_0^2)$ )	[—]		
$\alpha_C$	= dimensionless parameter ( $= C_{PS}/C_{PW}$ )	[—]		
$\alpha_K$	= dimensionless parameter ( $= K_S/K_W$ )	[—]		
$\alpha_T$	= dimensionless parameter ( $= K_w/(hr_0^2)$ )	[—]		
$\alpha_p$	= dimensionless parameter ( $= \rho_S/\rho_W$ )	[—]		
<Subscripts>				
$E$	= surrounding liquid			
$m$	= ultimate			
$0$	= initial value			

#### Literature Cited

- 1) Cussler, E. L., M. R. Stokar and J. E. Varberg: *AIChE J.*, **30**, 578 (1984).
- 2) Hirasa, O. *et al.*: in application for patent.
- 3) Hirokawa, Y., T. Tanaka and S. Katayama: "Microbial Adhesion and Aggregation," ed. by K. C. Marshall, p. 177 (1984).
- 4) Huang, X., H. Unno, T. Akehata and O. Hirasa: Preprints of the 51st Annual Meeting of The Soc. of Chem. Eng., Japan, p. 247 (1986).
- 5) Ogura, M.: *Kagaku Kougyou*, 137 (1984).
- 6) Tanaka, T. and D. J. Fillmore: *J. Chem. Phys.*, **70**, 1214 (1979).
- 7) Van Dijk, H. J. M., P. Walstra and J. Schenk: *Chem. Eng. J.*, **28**, B43 (1984).

## EFFECT OF CONTROLLED PULSATION ON AXISYMMETRIC JET BEHAVIOR

TADACHIKA SENO, SHIZUO KAGEYAMA AND RYUZO ITO

Department of Chemical Engineering, Osaka University, Toyonaka 560

**Key Words:** Fluid Mechanics, Axisymmetric Jet, Vortex Ring, Free Shear Layer, Strouhal Number, Eddy Reynolds Number, Hydrogen Bubble Method

Axisymmetric jets have been observed to investigate the effect of controlled pulsation on the behavior of vortex rings by using the hydrogen bubble technique and hot-film measurement. Pulsed jets had similar velocity profiles in the initial region and in the fully developed region. This similar velocity profile was coincident with that in natural jets. The differences between the two kinds of jets in volume rate, in decay of centerline velocity and in distribution of turbulent intensity, were observed to be remarkable in the initial region. Such differences were caused by the different behavior of vortex rings in the initial region. Behavior of vortex rings in the initial region of pulsed jets was roughly classified into three types by Strouhal number,  $Sr_0$  ( $Sr_0 < 0.9$ ,  $0.9 \leq Sr_0 < 2.6$ ,  $Sr_0 \geq 2.6$ ). It was found that the pulsation for  $Sr_0 = 0.3$  was the most dispersive wave in a jet column.

### Introduction

A number of studies on the large-scale structure in a circular jet have been carried out, especially in the initial region. The large-scale coherent structure plays key roles in the transport of heat, mass and momentum, and in the generation of aerodynamic noise. A circular jet is characterized by two length scales: the

characteristic thickness of the initial shear layer,  $\delta$ , and the jet diameter,  $D$ . The ratio  $\delta/D$  is a parameter controlling the characteristics and the evolution of large-scale structures in the axisymmetric shear layer. The effect of  $\delta/D$  on jet behavior was discussed in the previous paper.<sup>5)</sup>

Another parameter characterizing the large-scale structure is the velocity fluctuation in the shear layer near the nozzle exit. There have been two alternative approaches to the study of these structures. One is to study the naturally occurring ones.<sup>9,11)</sup> This approach

Received August 9, 1986. Correspondence concerning this article should be addressed to T. Seno. T. Seno and S. Kageyama are at College of Engineering, Shizuoka University, Hamamatsu 432.

has a number of constraints, primarily due to the large dispersion in shape, size, orientation, strength and convection velocity of these structures. The other is to study artificially excited ones. The controlled excitation triggers the formation of the structure at regular intervals and removes much of the jitter in the structure parameters. In most investigations, controlled excitation has been induced with the help of loudspeakers or spark generation, so that the amplitude of the pulsation is comparatively small. Details of large-scale structures in circular air jets in the narrow range of  $Sr_0$  at high  $Re$  ( $10^4$ – $5$  of order) have been reported by using the conditional sampling technique.<sup>3,4,10</sup>

In this study, growth of the pulsed jet was investigated by using the hydrogen bubble technique and hot-film measurement in a wide range of  $Sr_0$  at low  $Re$  ( $10^3$  of order). The amplitude of the pulsation on the efflux velocity is relatively large. In particular, the behavior of vortex rings (formation, coalescence, etc.) in pulsed jets is characterized in detail. Relating data obtained by hot-film measurements with those by flow visualizations is a useful method for conjecturing the structures of pulsed jets for various  $Sr_0$ . The clear visualization of formation and coalescence of vortex rings by the hydrogen bubble technique is expected to make contributions to the modeling of orderly large-scale structures in the free-shear layer.

## 1. Experimental Apparatus and Method

The experimental apparatus in this study is schematically shown in Fig. 1. A convergent nozzle of 2.15 cm exit diameter with an area contraction ratio of 21.6 was used. The tank into which a jet issued was 50 cm in width and depth, and 170 cm in length, so it was expected that the effect of tank walls on the behavior of vortex rings (formation, coalescence, etc.) could be ignored. The pump assembly was mounted on flexible neoprene mountings for isolating its vibrations. Velocity measurements were made by using a single hot-film sensor 0.15 mm in diameter, 3 mm in length with a constant-temperature anemometer and analog linearizer. Signals of the mean velocity and rms of velocity fluctuations from the anemometer set were recorded on a pen-recorder and signals of instantaneous velocity were recorded on a photocorder.

The hydrogen bubble technique was used for flow visualization. A platinum wire, 0.05 mm in diameter and 3 cm in length, was vertically placed across the nozzle exit plane. An electric pulse of 60–80 volts was periodically supplied to the wire to produce a sequence of time-lines of hydrogen bubbles as tracers. Photographs and video pictures were taken through the side wall of the tank by illuminating an axial slice of a jet with a stroboscope. The tank was darkened with black cloths to provide good contrast between

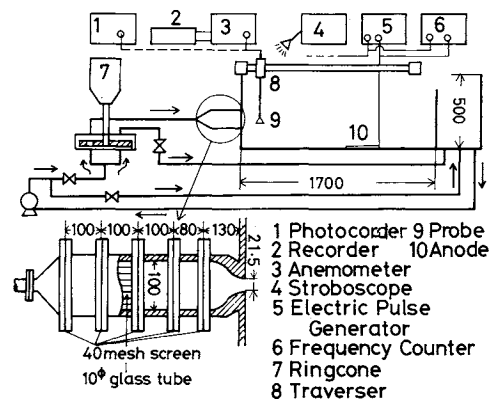


Fig. 1. Schematic diagram of experimental apparatus.

hydrogen bubbles and the background. The trajectory of a vortex ring was measured by using an X–Y tracker with a personal computer.

The pulsation on efflux velocity was made as follows. The fluid flowed into a thin cylindrical vessel from two inlets as shown in Fig. 2. A disk with three holes was rotating in the thin cylindrical vessel. The efflux velocity was larger when a hole in the rotating disk was overlapped with the outlet leading to the nozzle, whereas the efflux velocity was smaller when the outlet to the nozzle was obstructed by the wall of the rotating disk. For example, pulsed velocities on the centerline at the nozzle exit are shown in Fig. 3. The frequency of pulsation was controlled by the revolution speed of the disk. The amplitude of pulsation was controlled by changing the clearance between the rotating disk and the wall of the thin cylindrical vessel. The main operating conditions at the nozzle exit are shown in Table 1.

## 2. Experimental Results

### 2.1 Hot-film measurement

It is well known that velocity profiles at different sections in the initial region of a natural jet are similar. It was found that velocity profiles in the initial region of a pulsed jet were also similar. The velocity profile for pulsed jets was similar to that for natural jets and is expressed as follows:

$$\begin{aligned} U/U_0 &= 1.0 & r < r_c \\ U/U_0 &= 1/[1 + 0.414\{(r-r_c)/(r_h-r_c)\}^2]^2 & r \geq r_c \end{aligned} \quad (1)$$

Velocity profiles in the initial region for both kinds of jets are plotted in dimensionless form as  $U/U_0$  vs.  $(r_h-r)/(r_c-r_c)$  in Fig. 4. They agree reasonably well with Eq. (1). Velocity profiles in the fully developed region for both kinds of jets are plotted in dimensionless form as  $U/U_0$  vs.  $r/r_h$  in Fig. 5. Velocity profiles in the fully developed region for both kinds of jets were similar. The similar velocity profile in the fully developed region was also expressed as Eq. (1) with  $r_c=0$ .

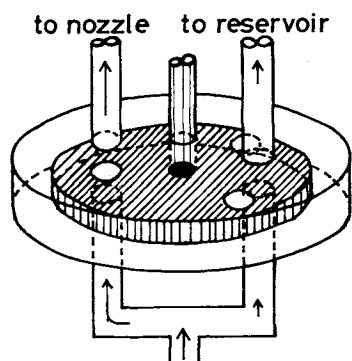


Fig. 2. Schematic diagram of fluid pulse generator.

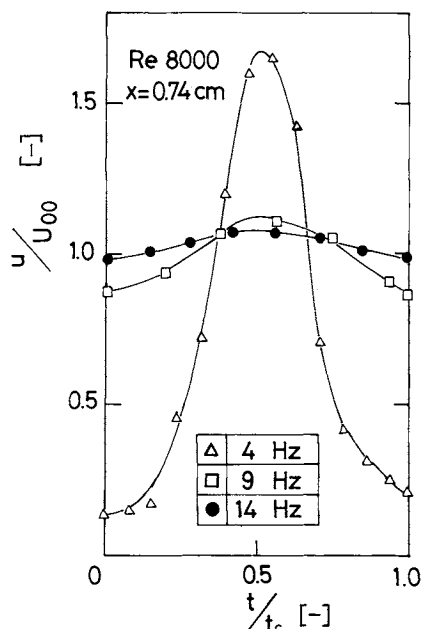


Fig. 3. Example of pulsed velocity.

Table 1. Experimental conditions at the exit

$Re$ [—]	$\Delta U_{00}/U_{00}$ [—]	$Sr_0$ [—]	$f_i$ [Hz]	$\sqrt{u'^2}/U_{00}$ [—]
2014	0.	—	—	0.004
1978	0.12	0.90	3.86	0.015
2014	0.087	1.65	7.21	0.015
1978	0.143	2.71	11.59	0.022
1895	0.124	4.13	16.92	0.019
1978	0.124	5.25	22.48	0.016
3968	0.	—	—	0.003
3968	0.159	0.45	3.86	0.048
3968	0.12	0.84	7.21	0.026
3968	0.234	1.35	11.59	0.058
3968	0.194	1.97	16.92	0.073
3968	0.199	2.62	22.48	0.052
6005	0.	—	—	0.003
6023	0.466	0.30	3.86	0.114
5958	0.230	0.56	7.21	0.161
6023	0.405	0.89	11.59	0.119
5981	0.342	1.31	16.92	0.095
5981	0.372	1.74	22.48	0.147

Figure 6 shows that dimensionless centerline velocities,  $U_0/U_{00}$ , are related to the dimensionless distance from the nozzle exit,  $X=x/D$ , over the

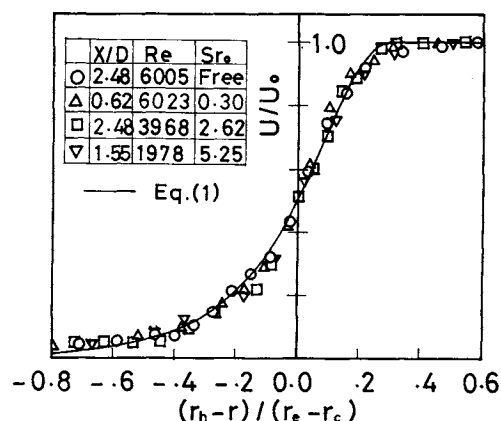


Fig. 4. Velocity profiles in the initial region.

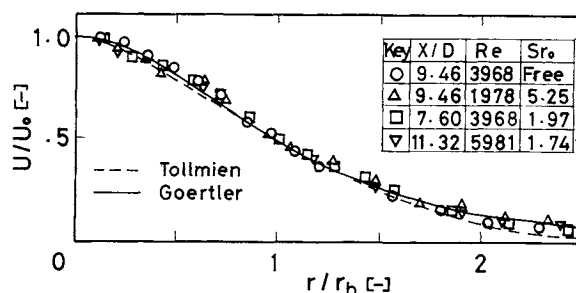


Fig. 5. Velocity profiles in the fully developed region.

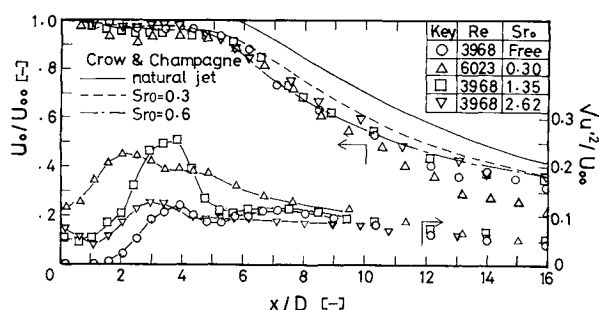


Fig. 6. Axial profiles of mean velocity and turbulent intensity on jet axis, normalized on the efflux velocity.

range  $0 < X \leq 16$ . For low  $Re$  of order  $10^3$ , centerline velocities of pulsed jets decreased once at  $X=1-2$  where shear layer rolled up to produce vortex rings, and then remained constant or increased slightly downstream up to the end of the potential core. They again decreased in inverse proportion to  $X$  in the fully developed region.

Virtual origins of jets,  $A_0$ , were determined by the gradients of centerline velocity decay, i.e., points at which lines of  $U_{00}/U_0$  intersect the  $x$  axis, and were located in the narrow range of  $X=1.8-2.2$  independent of  $Re$  and  $Sr_0$ . In the case of  $Sr_0=0.3$  alone, the virtual origin was located at about  $X=4$ . The spreading of the jet and the decay of the centerline velocity for  $Sr_0=0.3$  were more abrupt than those for the other  $Sr_0$ . This result seems to support the conclusion of Crow and Champagne<sup>1)</sup> that the preferred mode having a Strouhal number of 0.3 is in some

sense the most dispersive wave in a jet column, the wave least capable of generating a harmonic, and therefore the wave most capable of reaching a large amplitude before saturating.

**Figure 7** shows that dimensionless volume rates,  $Q/Q_0$ , are related to  $X$  together with the data of Crow and Champagne. Volume rates of pulsed jets increased more abruptly than those of natural ones in the range  $X < 3$ . It was found by flow visualization that vortex rings in pulsed jets formed closer to the nozzle exit and coalesced with adjacent ones more frequently than those in natural jets in that region. This result suggests that the coalescence of vortex rings plays a more important role in increasing the volume rate than does the viscosity of the fluid in that region. In the fully developed region, entrainment rates,  $dQ/dx$ , were almost constant independent of  $Sr_0$ .

Figure 6 shows that dimensionless turbulent intensities on the centerline of jets,  $\sqrt{u^2}/U_{00}$ , are related to  $X$  over the range  $0 < X \leq 16$ . In the region  $X < 1$ , where velocity fluctuations were caused by pulsation on efflux velocity at the nozzle exit, turbulent intensities decreased in the axial direction for  $Sr_0 > 0.45$ , whereas they increased for  $Sr_0 = 0.3$ . This result also seems to support the conclusion of Crow and Champagne. In the region  $1 < X < 5-6$ , where velocity fluctuations were caused by the formation, growth and coalescence of vortex rings, axial profiles of turbulent intensity depended on  $Sr_0$ . In the region  $X > 6$ , turbulent intensities decreased monotonously independent of  $Sr_0$ . The pulsation at the nozzle exit was of no effect.

## 2.2 Visualization of jets

Photographs of visualization of jets and an "x-t graph" are shown in **Figs. 8, 9 and 10**. X directional trajectories of vortex rings were measured from video pictures by using an X-Y tracker with a personal computer for about 3 seconds from an arbitrary time. They are shown in the "x-t graph" only in the range  $0 \leq t \leq 0.5$  or  $1.0$ . The x position and the frequency of vortex ring formation, of vortex ring coalescence and of vortex ring collapse and the transport velocity of vortex ring can be read from the "x-t graph". For example, x positions of vortex ring formation and of vortex ring coalescence were respectively coincident with the left end of vortex ring trajectory and with the junction of two vortex ring trajectories. The transport velocity of vortex ring was determined by the gradient of vortex ring trajectory. For a natural jet, the frequency and position of vortex ring formation depend on  $Re$ , and positions of vortex ring coalescence are random in the range  $1 < X < 3$  for  $1700 \leq Re \leq 8000$ .<sup>5)</sup> For a pulsed jet, generally speaking, the position of vortex ring formation was close to the exit,  $X < 1$ , independent of  $Re$  and  $Sr_0$ , and the

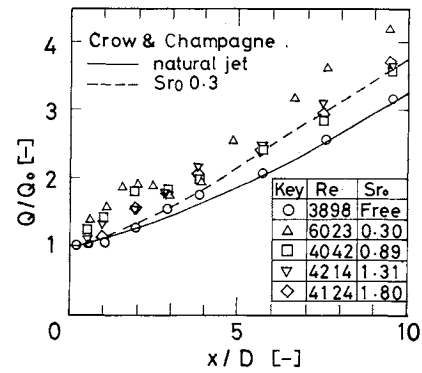


**Fig. 7.** Axial profiles of volume flux, normalized on the flux out the jet exit.

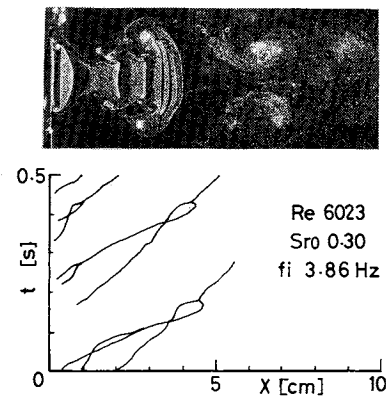


**Fig. 8.** Visualization of jet and trajectory of vortex ring.

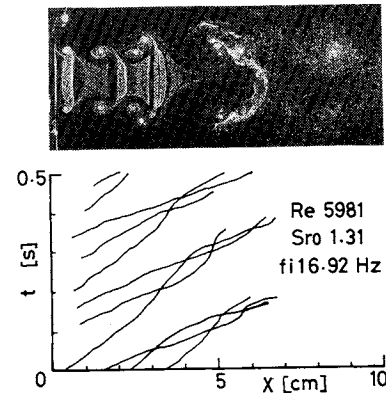


**Fig. 9.** Visualization of jet and trajectory of vortex ring.

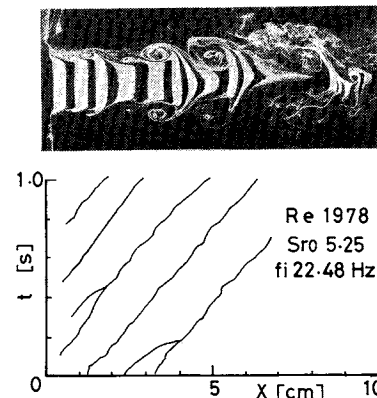


**Fig. 10.** Visualization of jet and trajectory of vortex ring.

position of vortex ring coalescence was fixed in the narrow range of  $X$ . The position of vortex ring coalescence,  $x_c$ , was correlated with  $Sr$  as  $x_c/D = 1.2Sr^{-1}$ . Petersen<sup>8)</sup> proposed  $x_c/D = Sr^{-1}$ . The transport velocity of vortex ring, normalized on the efflux velocity,  $U_v/U_{00}$ , is related to  $Sr_0$  in Fig. 11 together with data of Petersen.<sup>8)</sup> The mean value of  $U_v/U_{00}$  for natural jets was about 0.55, independent of  $Re$ . On the other hand,  $U_v/U_{00}$  of pulsed jets were 0.55–0.73, larger than those of natural jets. The present data were slightly larger than those of other authors<sup>2,8)</sup> for  $0.5 \leq Sr_0 \leq 2.0$ . With an increase of  $Sr_0$  over 4,  $U_v/U_{00}$  approached the value of 0.55, i.e., the value for the natural jet.

The behavior of vortex rings in the initial region of pulsed jets is summarized as follows.

A) For  $Sr_0 < 0.9$ , one pair of vortex rings, a larger one and a smaller one, was produced at the same periodic intervals as the pulsation. The larger vortex ring was induced by the pulsation at the exit, the smaller one by the fluctuation on the annular shear layer caused by the preceding larger one. It was often observed that two or three smaller induced vortex rings were following a larger one when the annular shear layer was thin, i.e., for larger  $Re$ . These small trailing vortex rings were engulfed in the larger preceding one and after coalescence the merged vortex ring disintegrated into turbulent eddies near the end of the initial region due to the entanglement of vortex core (cf. Fig. 8).

B) For  $0.9 \leq Sr_0 < 2.6$ , equal-sized vortex rings were produced distinctly at the same periodic intervals as the pulsation. The coalescence of three neighboring vortex rings or double coalescences (four vortex rings were concerned) or the “slip through” phenomenon was observed (cf. Fig. 9).

C) For  $Sr_0 \geq 2.6$ , vortex rings were produced independently of  $Sr_0$ . The frequency and position of the coalescence of vortex rings became irregular just as for a natural jet. But the position of vortex ring formation was closer to the exit than that in a natural jet (cf. Fig. 10).

When the amplitude of the pulsation was large, more clearly distinct vortex rings were produced, and a little effect of the pulsation amplitude on the position of vortex ring formation was observed. No effect of the amplitude on the frequency of vortex ring formation or the pattern of vortex ring coalescence was observed.

### 3. Discussion

Relating data obtained by hot-film measurements with those by flow visualizations is a useful method for understanding the characteristics of pulsed jets for various  $Sr_0$ . For example, the combination of flow visualization with hot-film measurement for  $Sr_0 =$

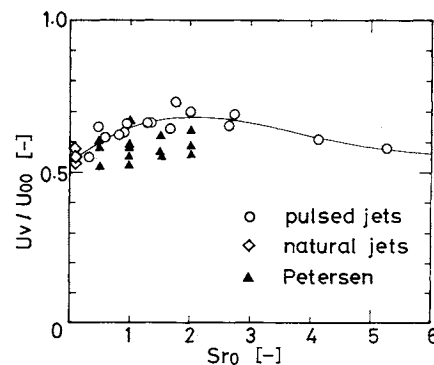


Fig. 11. Mean transport velocity of vortex ring for various  $Sr_0$ .

0.45 and  $Re = 3968$  is shown in Fig. 12. The bottom figure in Fig. 12 shows the contour of turbulent intensity. Numbers in the figure denote  $\sqrt{u'^2}/U_{00} \times 100\%$ . In the region  $X < 1.5$ , where axisymmetric vortex rings were produced, grew and then coalesced, the volume rate increased abruptly by engulfing the ambient fluid in the process of coalescence. On the other hand, the centerline velocity decreased by the momentum transfer from the potential core to vortex rings in the shear layer. In the region  $1.5 < X < 5$ , where large and merged vortex rings were swept downstream and wave deformations of cores of vortex rings were growing with increasing  $X$ , the volume rate increased slightly and centerline velocity remained constant. In the region  $X > 5$ , where vortex rings disintegrated into turbulent eddies due to the entanglement of distorted vortices and no orderly structure was observed, the volume rate increased again and the centerline velocity decreased inversely proportionally to  $X + A_0$ . The region where the intensity of turbulent fluctuation had a large value was coincident with the region where vortex rings coalesced or collapsed.

Petersen used the parallel stability theory of Michalke<sup>7)</sup> and Mattingly<sup>6)</sup> to estimate the local dispersion relation as a function of downstream distance. Our result is compared with that of Petersen in Fig. 13. The solid curve is based on the Michalke theory, the broken curve on that of Mattingly. Together the loci define a dispersive boundary. Our result seems to support the conclusion of Petersen that the first pairing occurs where the mixing layer becomes sufficiently thick, owing to nonlinearities and entrainment, and that a subharmonic wave has a phase velocity that matches the convection speed of the vortex rings.

### Conclusion

1) Pulsed jets for various  $Sr_0$  have the same similar velocity profile in the initial region and in the fully developed region. This similar velocity profile is

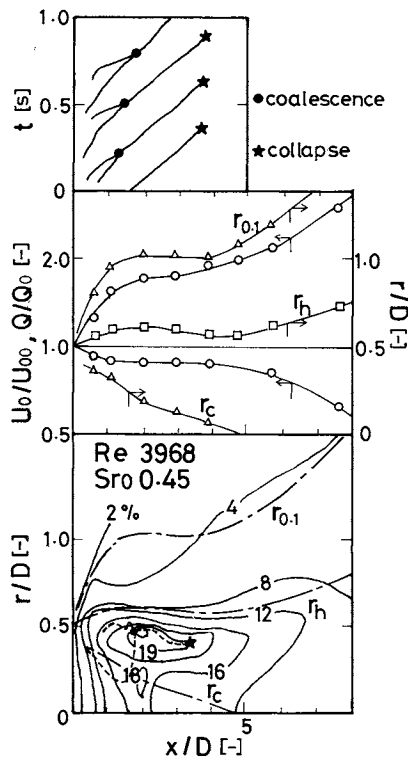


Fig. 12. Combination of hot-film measurement with flow visualization.

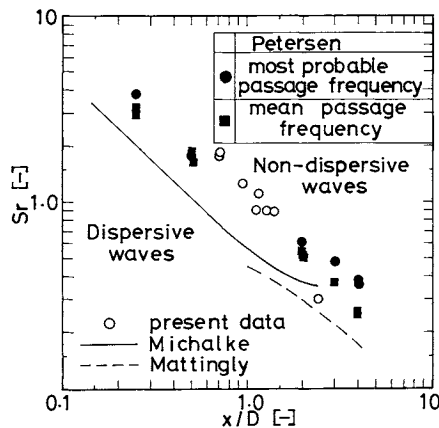


Fig. 13. Relation of  $Sr$  based on passage frequency to  $x/D$ .

coincident with that in natural jets and is expressed as Eq. (1).

2) Differences between pulsed jets and natural ones in volume rate, in decay of centerline velocity and in distribution of turbulent intensity are observed to be remarkable in the initial region. For example, volume rates of pulsed jets increase more abruptly than those of natural ones in the region of  $X < 3$ . Such differences are caused by the different behavior of vortex rings in the initial region. In the fully developed region, however, such differences disappear.

3) Behavior of vortex rings in pulsed jets is roughly classified into three types by  $Sr_0$  (i.e.,  $Sr_0 < 0.9$ ,  $0.9 \leq Sr_0 < 2.6$ ,  $Sr_0 \geq 2.6$ ).

4) In the case of  $Sr_0 = 0.3$ , the centerline velocity decreases more abruptly and the volume rate increases more abruptly than those in the other cases in the initial region. In the region  $X < 1$ , the turbulent intensity on the centerline of the jet increases in the axial direction for  $Sr_0 = 0.3$ , whereas it decreases for the other  $Sr_0$ . These results support the observation that the wave for  $Sr_0 = 0.3$  is the most dispersive one in a jet column.

#### Nomenclature

$A_0$	= virtual origin	[m]
$D$	= diameter of nozzle exit	[m]
$f$	= mean passage frequency of vortex	[Hz]
$f_i$	= frequency of pulsation	[Hz]
$Q$	= volume rate	[m <sup>3</sup> s <sup>-1</sup> ]
$Q_0$	= volume rate at nozzle exit	[m <sup>3</sup> s <sup>-1</sup> ]
$Re$	= $\rho D U_{00} / \mu$ , Reynolds number	[—]
$r$	= radial distance from jet axis	[m]
$r_c$	= $r$ at which velocity is $0.97 U_0$	[m]
$r_e$	= $r$ at which velocity is $0.05 U_0$	[m]
$r_h$	= $r$ at which velocity is $0.5 U_0$	[m]
$r_0$	= radius of nozzle exit	[m]
$r_{0.1}$	= $r$ at which velocity is $0.1 U_0$	[m]
$Sr$	= $f D / U_{00}$ , Strouhal number	[—]
$Sr_0$	= $f_i D / U_{00}$ , Strouhal number	[—]
$t$	= time	[s]
$t_c$	= period of pulsation	[s]
$U$	= mean velocity	[m s <sup>-1</sup> ]
$U_v$	= mean transport velocity of vortex ring	[m s <sup>-1</sup> ]
$U_0$	= mean velocity on jet axis	[m s <sup>-1</sup> ]
$U_{00}$	= mean velocity at nozzle exit	[m s <sup>-1</sup> ]
$\Delta U_{00}$	= difference between maximum velocity and minimum velocity of pulsation	[m s <sup>-1</sup> ]
$u$	= instantaneous velocity	[m s <sup>-1</sup> ]
$u'$	= velocity fluctuation	[m s <sup>-1</sup> ]
$X$	= $x/D$ , dimensionless axial distance	[—]
$x$	= axial distance from exit	[m]
$x_c$	= $x$ position of vortex ring coalescence	[m]
$\delta$	= thickness of shear layer at exit	[m]
$\mu$	= viscosity of fluid	[Pa · s]
$\rho$	= density of fluid	[kg · m <sup>-3</sup> ]

#### Literature Cited

- 1) Crow, S. C. and F. H. Champagne: *J. Fluid Mech.*, **48**, 547 (1971).
- 2) Heavens, S. N.: *J. Fluid Mech.*, **100**, 185 (1980).
- 3) Hussain, A. K. M. F., S. J. Kleis and M. Sokolov: *J. Fluid Mech.*, **98**, 97 (1980).
- 4) Hussain, A. K. M. F. and K. B. M. Q. Zaman: *J. Fluid Mech.*, **110**, 39 (1981).
- 5) Ito, R. and T. Seno: *J. Chem. Eng. Japan*, **12**, 430 (1979).
- 6) Mattingly, G. E. and C. C. Chang: *J. Fluid Mech.*, **65**, 541 (1974).
- 7) Michalke, A.: *Z. Flugwiss.*, **19**, 319 (1971).
- 8) Petersen, R. A.: *J. Fluid Mech.*, **89**, 469 (1978).
- 9) Ribeiro, M. M. and J. H. Whitelaw: *J. Fluid Mech.*, **70**, 1 (1975).
- 10) Sokolov, M., A. K. M. F. Hussain, S. J. Kleis and Z. D. Husain: *J. Fluid Mech.*, **98**, 65 (1980).
- 11) Yule, A. J.: *J. Fluid Mech.*, **89**, 413 (1978).